Cement and Concrete Research 40 (2010) 1255–1264

Contents lists available at ScienceDirect

Cement and Concrete Research

journal homepage: http://ees.elsevier.com/CEMCON/default.asp

Modeling experimental results of diffusion of alkaline solutions through a compacted bentonite barrier

Raúl Fernández [a,c,*], Jaime Cuevas [b], Urs K. Mäder [c]

[a] Instituto Eduardo Torroja de Ciencias de la Construcción (CSIC), C/Serrano Galvache, 4, 28033 Madrid, Spain
[b] Dpto. Geología y Geoquímica, Facultad de Ciencias, Universidad Autónoma de Madrid, Campus Cantoblanco, 28049 Madrid, Spain
[c] Institut für Geologie, Universität Bern, Baltzerstrasse 3, CH-3012 Bern, Switzerland

ARTICLE INFO

Article history:
Received 13 May 2009
Accepted 16 September 2009

Keywords:
Kinetics (A)
Diffusion (C)
Radioactive waste (E)
Modeling (E)
Bentonite

ABSTRACT

The interaction between concrete/cement and swelling clay (bentonite) has been modeled in the context of engineered barrier systems for deep geological disposal of high-level radioactive waste. The geochemical transformations observed in laboratory diffusion experiments at 60 and 90 °C between bentonite and different high-pH solutions (K–Na–OH and $Ca(OH)_2$-saturated) were reconciled with the reactive transport code CrunchFlow. For K–Na–OH solutions (pH = 13.5 at 25 °C) partial dissolution of montmorillonite and precipitation of Mg-silicates (talc-like), hydrotalcite and brucite at the interface are predicted at 60 °C, while at 90 °C the alteration is wider. Alkaline cations diffused beyond the mineralogical alteration zone by means of exchange with Mg^{2+} in the interlayer region of montmorillonite. Very slow reactivity and minor alteration of the clay are predicted in the $Ca(OH)_2$-bentonite system. The model is a reasonable description of the experiments but also demonstrates the difficulties in modeling processes operating at a small scale under a diffusive regime.

1. Introduction

Concrete and compacted bentonite are being studied as components of engineered barrier systems to isolate high-level radioactive waste in geological disposal. These materials should conserve the physical and chemical characteristics for what they have been designed until the radioactive waste and the spent nuclear fuel decrease their radioactivity levels to near the natural background. However, both materials will evolve over time due to their different compositions. The high-pH (13–14) fluids emanating from OPC-type concrete will interact with the bentonite barrier where these two materials will be placed in direct contact. The initial composition of the concrete porewater is dominated by K^+ (0.2–0.5 M), Na^+ (0.05–0.2 M) and OH^- (0.3–0.7 M), and will evolve to Ca-$(OH)_2$ solutions after the alkali-leaching period [1–3]. At laboratory scale these situations are simulated with two types of synthetic alkaline solutions: an early cement water, mainly Na–K–OH with pH ~13.5 at 25 °C, used to simulate early repository conditions, and an Evolved Cement Water, saturated with respect to portlandite (pH ~12.5, at 25 °C), that represents the conditions expected to prevail for a very long time in a repository. The duration for which the barrier should conserve its retention properties for radionuclides is 10^5 to 10^6 years.

Numerous laboratory experiments [4–13], natural analogues [14–19] and modeling studies [20–26] confirm and detail the alteration of clays by interaction with alkaline fluids. These studies agree on the following processes related to cement/bentonite systems:

1. Concrete or cement (Ordinary Portland Cement: OPC) reacts initially with bentonite due to the high-pH porewater. Montmorillonite dissolves under hyperalkaline conditions, precipitating zeolites and leaving a Mg-rich residual clay.
2. Bentonite is able to buffer the hyperalkaline pH (13.6–13.0, for OPC) to pH ≤ 12.5. Portlandite is then slowly dissolved at the interface, forming C–S–H gels (Ca–Si-hydrate). Crystalline C–S–H gels of tobermorite-type form at temperature higher than 80 °C at laboratory time scales.
3. Some of the dissolved Ca^{2+} is incorporated in the exchangeable complex of bentonite, displacing Mg^{2+}, which precipitates as brucite [$Mg(OH)_2$] or hydrous magnesium silicate and hydrotalcite depending on the temperature of reaction.

Diffusion experiments with alkaline solutions and compacted bentonite columns show the coupling between the changing porosity due to cementation processes at the interface, and the retardation of alteration in the cemented layer, as well as the decrease in the cation exchange capacity of bentonite due to montmorillonite dissolution as the main geochemical reactions [27]. The reactive transport geochemical code CrunchFlow is used in this study to investigate numerically the same system, with the aim to reproduce the alteration reactions observed experimentally with special focus on

* Corresponding author. Mailing Address: Instituto Eduardo Torroja de Ciencias de la Construcción (CSIC), C/Serrano Galvache 4, 28033 Madrid, Spain. Tel.: +34 913020440x242; fax: +34 913020700.
E-mail address: raul.fernandez@ietcc.csic.es (R. Fernández).

0008-8846/$ – see front matter © 2009 Elsevier Ltd. All rights reserved.
doi:10.1016/j.cemconres.2009.09.011

cation exchange and mineralogical transformations in order to confirm and clarify key processes, and provide insight into expected system behaviour over long periods of time. In order to achieve relevant results that permit the interpretation of the experimental observations, some of the key parameters were selected based on available published data but some others were adjusted to obtain numerical convergence (reaction rates, diffusion coefficients, etc.).

2. Experimental conditions and main results

The experimental system consists of a cylindrical compacted bentonite column in contact with a 0.6 M $MgCl_2$ solution at one end and a synthetic alkaline solution at the other end of the column (Fig. 1). To maintain an almost constant source of alkalinity, the alkaline solution is constantly circulated from a 0.5 L solution reservoir by a peristaltic pump. No circulation was applied to the $MgCl_2$ solution since the only objective was to maintain saturated conditions during the course of the experiment. A set of 12 experiments were performed under these conditions over 6, 12 and 18/24 months, applying a constant temperature of 60 °C (6, 12, 24 months) and 90 °C (6, 12, 18 months), and using 2 different alkaline solutions: Young Cement Water (YCW) and Evolved Cement Water (ECW).

The clay material was pre-treated to saturate the exchangeable complex of montmorillonite in Mg^{2+}; but the mineralogical composition of bentonite was not modified. Most soluble salts, such as gypsum or halite, were washed out from the bulk clay during the saturation process but some calcite remained in bentonite after Mg-saturation. This pre-treatment permits to study the mineralogical transformations in the first millimeters of the alkaline interface since exchangeable Mg^{2+} is displaced from the interlayer of montmorillonite under alkaline conditions, precipitating as brucite or incorporating itself in the internal structure of silicates in a non-exchangeable form [7,13,28].

At 60 °C, diffusion of the hyperalkaline plume (YCW: K/NaOH solution) through compacted bentonite (1.6 g/cm^3 dry density) produced a domain of mineralogical alteration characterized by a cemented rim of 2 mm thickness, developed in 6 months. The thickness of alteration did not evolve thereafter despite the nearly constant input solution composition owing to an increased surface area and reduced porosity that caused a strong retardation of diffusion. Montmorillonite was partially dissolved and formation of brucite, Al- and Mg-chlorite-type silicates were observed within this domain. XRD diffraction suggests intercalation of hydroxides and hydrotalcite-type structures (7.5 Å). Zeolites were not observed.

At 90 °C, the alteration zone had a larger extent, and this was observed as a hardening of the bentonite column and partial occlusion of the connected porosity, retarding the diffusion of alkaline cations. Only traces of analcime were detected at the interface with the YCW.

The pH was buffered efficiently by montmorillonite dissolution at 60 and 90 °C as evidenced by only small amounts of brucite precipitation. Brucite would be the main secondary phase if pH was maintained at the initial value. Disturbance of the ion exchange complex extended deeper than the mineralogical alteration; substitution of Mg^{2+} by K^+ was detected even at 60 °C and after 6 months along the entire column of bentonite (2.1 cm).

Further details of the experiments are reported in [27].

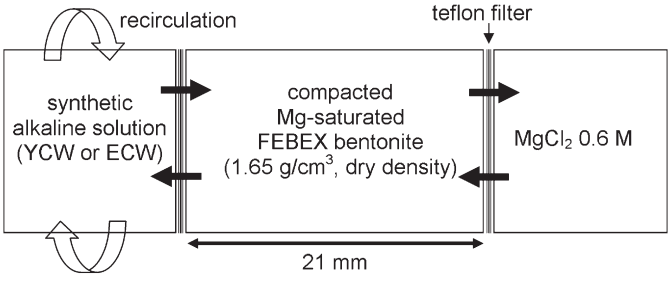

Fig. 1. Experimental set-up of diffusion experiments.

3. Physical model and approach

Modeling was carried out using the geochemical computer code CrunchFlow [29–31] that can be operated in two modes: using the Sequential Iteration Approach (SIA) which solves the transport and chemical equations sequentially, or the Direct Substitution Approach (DSA) which solves the transport and chemical equations simultaneously. Geochemical evolution in CrunchFlow is modeled using user-defined kinetic rate laws for mineral reactions, and chemical equilibrium for aqueous speciation and surface reactions. The code takes into account aqueous speciation, mineral dissolution/precipitation, surface complexation, ion exchange, and transport processes. Transport in the system may optionally be coupled to or decoupled from the evolving porosity when minerals precipitate or dissolve. Aqueous species can be constrained by mineral or gas equilibrium and charge balance. Reactions given in the database are temperature dependent extending up to 300 °C but several inconsistencies had to be resolved and supplementary data supplied (see details below).

In analogy to the laboratory experiments, the model considers an alkaline solution (either YCW or ECW; Table 1) diffusing through the bentonite column, which is divided into 21 cells of 1 mm each, with the same initial mineralogical composition and porewater composition (Table 2). The alkaline solution is located outside the column, adjacent to the bentonite domain. At the end of the column, 2 cells of 1 mm are added for a 0.6 M $MgCl_2$ solution. The transport is limited to diffusive interaction between the infinite source of alkalinity and the bentonite and $MgCl_2$ domains. Mineral dissolution/precipitation, aqueous speciation and ion exchange selectively associated to montmorillonite are the geochemical processes included in all scenarios. The DSA mode was used in this study which will allow for larger time stepping and better performance.

3.1. Initial considerations

A model in one dimension was preferred due to the approximate homogeneity of the domains involved in the system and for simplicity in order to express the results as a function of distance from the alkaline interface.

Watson et al. [32] performed predictive modeling of the diffusion of cementitious water in bentonite with a sensitivity study of input parameters, using the code Raiden-3 [33]. They observed different behaviours in the system as a function of the size of the alkaline reservoir. The larger the reservoir, the longer it took for montmorillonite dissolution to start, but when it did it was at a faster dissolution rate. For an infinite reservoir, montmorillonite dissolution started before other cases examined and was more rapid. A dependency on the alkaline reservoir size is also observed in this study with CrunchFlow; but the alkaline fluid has been considered an infinitely large reservoir out of the domain. This fact disagrees with the

Table 1
Synthetic concrete porewater compositions (mol/kg solution).

Aqueous species	YCW	ECW
OH^- (charge balance)	4.27E−2	4.00E−2
K^+	3.54E−1	
Na^+	1.02E−2	
Ca^{2+}	7.36E−4	2.00E−2
SO_4^{2-}	1.53E−2	
$O_{2(aq)}$	1.00E−8	1.00E−8
pH	12.4 (60 °C) 11.8 (90 °C)	11.447 (60 °C)

Table 2
Mineralogical and chemical compositions of the bentonite column.

Mineral	% wt.	Aqueous species	Concentration (mol/kg solution)
Albite	1	OH^-	3.1E−7
Calcite	1	K^+	1.2E−5
Cristobalite-α	2	Na^+	1.0E−3
Illite	1	Ca^{2+}	1.2E−4
K-feldspar	1	Mg^{2+}	6.0E−1
Mg-montmor-FEBEX	92	Al^{3+}	1.3E−7
Quartz	2	Fe^{2+}	1.0E−8
		$O_{2(aq)}$	1.0E−12
		SO_4^{2-}	6.3E−5
		Cl^- (charge balance)	7.92E−1 (60 °C) 9.39 (90 °C)
		HCO_3^- (eq. with calcite)	4.08E−1 (60 °C) 2.62E−1 (90 °C)
		$SiO_{2(aq)}$	3.9E−6

experiment, where the mass of alkaline solution was constrained to 0.5 kg and dissolved species present in the bentonite porewater could have entered the solution reservoir. While the solution chemistry of the reservoir was not monitored, pH measurements confirm the stability of the alkaline solution, showing a performance close to the infinite reservoir case.

Cation exchange capacity (CEC) is a relevant parameter to study in the model because it is directly related to the mineralogical alteration. This property was tied exclusively to the mineral phase Mg-montmor-FEBEX, and therefore, the partial dissolution of this mineral in the first millimeters of bentonite at the alkaline side will produce a proportional decrease in the CEC. Although some minor inconsistencies were detected in the analytical determination of exchangeable cations (excess of Ca^{2+} and Mg^{2+} were measured due to dissolution of calcite and amorphous phases during extractions), the correlation of montmorillonite dissolution and CEC decrease was clearly observed experimentally at the interface. Secondary minerals such as zeolites and clays, which are often considered as cation exchangers, form a negligible contribution in this particular system as was demonstrated by [13], and therefore, they were not considered as exchangers in the model. Cation exchange coefficients for Mg-montmorillonite were selected from [34], who studied the ion exchange behaviour of the smectite used experimentally in this study.

Porosity is a key parameter to be estimated in the model since it regulates the solid:solution ratio, the solute concentrations and therefore also the reaction rates. In smectite-type clays, 3 types of porosity can be considered for solute transport: (1) *free porosity* (or *free porewater*) is the water without electrostatic interactions that connect the porosity in the system (these two terms are equivalent when bentonite is fully saturated, as in this case), (2) *interlamellar water* is the porosity available in the interlayer space of smectite, and (3) space occupied by the diffuse double layer surrounding the external surfaces of clay particles [35]. These latter two regions are preferentially accessible for cations that compensate the negative net charge of clay surfaces. CrunchFlow does not differentiate between these types of porosity; but it is able to allow diffusive transport of aqueous species at species-specific rates while conserving electro neutrality by imposing electrochemical migration terms. Water vapour adsorption/desorption isotherms, together with *c*-lattice spacing determinations performed on bentonite indicate that most of the water resides in the interlayer [36], particularly at dry densities higher than 1.4 g/cm^3 [37]. In this study cation migration through the montmorillonite interlayer is dominant due to the high degree of compaction (1.65 g/cm^3 dry density). Initial total porosity is assumed as 40% of the total volume based on water-content measurements and the sum of minerals as 60% by difference. Diffusion of all species is dependent on the available porosity at any time, and therefore, a decrease in porosity caused by precipitation of secondary minerals produced a decrease in diffusive transport of aqueous species. The fast movement of exchangeable K^+ and Na^+ along the column observed experimentally can only be predicted by forcing cations to migrate faster than anions.

Two types of parameters have been modified at 90 °C with respect to the model at 60 °C: (1) the diffusion coefficient of aqueous species and (2) the dependency of reaction rate on pH.

3.2. Diffusion coefficients

Specific diffusion coefficients have been considered for each aqueous species, calculated based on the diffusion coefficients for ions in free water [38,39] but reduced by several orders of magnitude to obtain pore diffusion coefficients compatible with measurements in bentonite compacted at high density (reduction of free porewater, increase of tortuosity, etc.). These coefficients agree with [9], who established that, for a given clayey material, effective diffusion coefficients (*De*) for the cations K^+, Ca^{2+}, Na^+ and Cs^+ are in the same order of magnitude, but *De* for Cl^- is one to two orders of magnitude lower. This is a simplification of a more mechanistic treatment of anion exclusion effects (e.g., [35]).

The diffusive fluxes (J) for aqueous species increase with temperature according to the 1st Fick law:

$$J = -D\left(\frac{\partial x}{\partial C}\right);\ D = D_{25}e^{\left[\frac{-E_a}{R}\left(\frac{1}{T}-\frac{1}{298.15}\right)\right]} \quad (1)$$

where D is the diffusion coefficient of each species at the working temperature and D_{25} is the diffusion coefficient of the aqueous species at 25 °C. D_{25} values have been specified for the relevant species, assigning a generic value for all other species (D_0). Increase of temperature takes implicitly an increase of diffusion coefficients into account except for the generic value that was manually adjusted upwards, from 60 to 90 °C, by a factor of 3 to better fit the experimental observations (Table 3).

4. Thermodynamic and kinetic data

27 aqueous species (Table 4) and 20 minerals (Tables 5 and 6) have been taken into account in this study. Most of the aqueous species of interest are included in the default database of CrunchFlow (datacom), which is an adaptation of the EQ3/6 database in the required format. However, due to the absence of some relevant species at high pH and inconsistencies found in comparison with other databases for a few other species (work in progress), the program SUPCRT92 in addition to its updated default database SLOP98 was used to estimate the equilibrium constants at the required temperatures for $CaHSiO_3^+$, $CaOH^+$, $CO_{2(aq)}$, CO_3^{2-}, KOH, $MgOH^+$, $NaHSiO_3$ and NaOH. Equilibrium constants and their temperature dependence for the species $H_2SiO_4^{2-}$ and $NaSO_4^-$, which had no

Table 3
Diffusion coefficients at 25, 60 and 90 °C in bentonite porewater.

Aqueous species	D_{25}	D_{60}	D_{90}
H^+	9.31E−11	2.26E−10	4.22E−10
Na^+	1.33E−11	3.23E−11	6.03E−11
K^+	1.96E−11	4.76E−11	8.88E−11
Mg^{2+}	0.71E−11	1.71E−11	3.20E−11
Ca^{2+}	0.79E−11	1.93E−11	3.59E−11
Al^{3+}	0.56E−11	1.36E−11	2.53E−11
Cl^-	1.10E−12	2.67E−12	4.99E−12
SO_4^{2-}	1.07E−12	2.60E−12	4.85E−12
HCO_3^-	1.18E−12	2.87E−12	5.35E−12
$SiO_{2(aq)}$	2.20E−12	5.34E−12	9.97E−12
Generic (D_0)	1.00E−11	2.43E−11	–
Generic (D_0)	3.00E−11	–	1.36E−10

Table 4
Aqueous reactions and equilibrium constants used in this study.

Aqueous reaction	log *k* (25 °C)	log *k* (60 °C)	log *k* (90 °C)
$AlO_2^- + 4\,H^+ = Al^{3+} + 2\,H_2O$	22.88	19.57	16.83
$AlOH^{2+} + H^+ = Al^{3+} + H_2O$	4.96	4.00	3.32
$Al(OH)_2^+ + 2\,H^+ = Al^{3+} + 2\,H_2O$	10.59	8.75	7.32
$CaCO_{3(aq)} + H^+ = Ca^{2+} + HCO_3^-$	7.00	6.45	6.05
$CaHCO_3^+ = Ca^{2+} + HCO_3^-$	−1.05	−1.16	−1.41
$CaHSiO_3^+ + H^+ = Ca^{2+} + SiO_{2(aq)} + H_2O$	8.58	8.12	7.75
$CaOH^+ + H^+ = Ca^{2+} + H_2O$	12.83	11.42	10.36
$CaSO_{4(aq)} = Ca^{2+} + SO_4^{2-}$	−2.11	−2.26	−2.47
$CO_{2(aq)} + H_2O = H^+ + HCO_3^-$	−6.34	−6.27	−6.28
$CO_3^{2-} + H^+ = HCO_3^-$	10.33	10.13	10.08
$H_2SiO_4^{2-} + 2\,H^+ = SiO_{2(aq)} + 2\,H_2O$	23.00	21.64	20.69
$HSiO_3^- + H^+ = SiO_{2(aq)} + H_2O$	9.95	9.47	9.17
$KCl_{(aq)} = K^+ + Cl^-$	1.49	1.22	1.00
$KOH_{(aq)} + H^+ = K^+ + H_2O$	14.44	13.31	12.50
$KSO_4^- = K^+ + SO_4^{2-}$	−0.88	−0.99	−1.16
$MgCl^+ = Mg^{2+} + Cl^-$	0.13	0.05	−0.12
$MgCO_{3(aq)} + H^+ = Mg^{2+} + HCO_3^-$	7.35	6.93	6.59
$MgHCO_3^+ = Mg^{2+} + HCO_3^-$	−1.04	−1.16	−1.33
$MgOH^+ + H^+ = Mg^{2+} + H_2O$	11.68	10.50	9.60
$MgSO_{4(aq)} = Mg^{2+} + SO_4^{2-}$	−2.41	−2.84	−3.17
$NaCl_{(aq)} = Na^+ + Cl^-$	0.78	0.65	0.55
$NaCO_3^- + H^+ = Na^+ + HCO_3^-$	9.81	10.07	10.39
$NaHCO_{3(aq)} = Na^+ + HCO_3^-$	−0.15	0.11	0.34
$NaHSiO_{3(aq)} + H^+ = Na^+ + SiO_{2(aq)} + H_2O$	7.76	7.77	7.76
$NaOH_{(aq)} + H^+ = Na^+ + H_2O$	14.21	13.21	12.51
$NaSO_4^- = Na^+ + SO_4^{2-}$	−0.70	−0.79	−0.85
$OH^- + H^+ = H_2O$	14.00	13.03	12.35

Values at 25 °C are given as reference but not used in the models.

temperature dependence in the default database, were taken from the database of PHREEQC.

Seven primary minerals were selected to define the initial composition of bentonite. Mg-montmor-FEBEX (92% in weight) has a composition based on the phase FEBEX-montmorillonite [40] where the exchangeable cations Na^+, K^+ and Ca^{2+} were all replaced by Mg^{2+}, assuming the same chemical stability. Exchangeable reactions and selectivity coefficients applied for cation exchanges in the interlayer region of montmorillonite were considered as in [40], using the Vanselow convention.

Albite, calcite, cristobalite-α, illite, K-feldspar and quartz were included as accessory minerals. Soluble minerals were not considered due to the pre-treatment performed, where it is assumed that these minerals dissolved. Thirteen secondary minerals were taken into account as possible results of mineralogical transformations, seven of them imported from the thermodynamic database THERMODDEM (http://thermoddem.brgm.fr; see Table 5). Brucite, hydrotalcite, a chlorite-like phase and gibbsite were experimentally observed as well as a secondary Mg-enriched-clay for which saponite-Mg and talc were considered as a proxy. Additionally, phillipsite has been included as zeolite, although experimental evidences do not confirm its formation. C–S–H gels, portlandite, ettringite and tobermorite-11 Å were considered as secondary cement phases.

The rate equations for the dissolution/precipitation of all minerals considered in this work apply to the transition state theory, described by [45,46] and [47] as:

$$r_m = A_m k(T)(a_{H^+})^n \left[1 - \left(\frac{Q_m}{K_m}\right)\right] \quad (2)$$

where r_m is the dissolution/precipitation rate of the mineral m ($mol \cdot m^{-3} \cdot s^{-1}$), A_m is the specific mineral surface area (m^2 mineral m^{-3} porous medium), $k(T)$ is the temperature dependent rate constant ($mol \cdot m^{-2} \cdot s^{-1}$), $(a_{H^+})^n$ is the proton activity raised to the power n (which is a value experimentally determined), K_m is the equilibrium constant for the dissolution reaction of the mineral m, and Q_m is the ion activity product for this reaction.

The dependence of the rate constant on temperature is defined as:

$$k(T) = k_{25} \exp\left[\frac{-E_a}{R}\left(\frac{1}{T} - \frac{1}{298.15}\right)\right] \quad (3)$$

where k_{25} is the rate constant of mineral m at 25 °C ($mol \cdot m^{-2} \cdot s^{-1}$), E_a is the activation energy of reaction ($kcal \cdot mol^{-1}$), R is molar gas constant ($kcal \cdot K^{-1} \cdot mol^{-1}$) and T is the absolute temperature (K).

Table 5
Thermodynamic data and dissolution reaction of the selected minerals adopted in the models.

Mineral	Reaction	log *k* (25 °C)	log *k* (60 °C)	log *k* (90 °C)	Molar volume ($cm^3 \cdot mol^{-1}$)
Albite	$NaAlSi_3O_8 + 4H^+ \leftrightarrow Al^{3+} + Na^+ + 3SiO_{2(aq)} + 2H_2O$	2.76	1.57	0.63	100.25
Calcite	$CaCO_3 + H^+ \leftrightarrow Ca^{2+} + HCO_3^-$	1.85	1.33	0.91	36.93
Cristobalite-α	$SiO_2 \leftrightarrow SiO_{2(aq)}$	−3.45	−2.99	−2.67	25.74
Illite	$K_{0.6}Mg_{0.25}Al_{2.3}Si_{3.5}O_{10}(OH)_2 + 8H^+ \leftrightarrow 0.25Mg^{2+} + 0.6\,K^+ + 2.3Al^{3+} + 3.5SiO_{2(aq)} + 5H_2O$	9.03	5.56	2.75	138.94
K-feldspar	$KAlSi_3O_8 + 4H^+ \leftrightarrow Al^{3+} + K^+ + 3SiO_{2(aq)} + 2H_2O$	−0.28	−0.96	−1.56	108.87
Mg-montmor-FEBEX	$Mg_{0.32}(Al_{1.545}Mg_{0.425})(Si_{3.86}Al_{0.145})O_{10}(OH)_2 + 6.56H^+ \leftrightarrow 0.745Mg^{2+} + 1.69Al^{3+} + 3.86SiO_{2(aq)} + 4.28H_2O$	6.26	4.23	2.56	134.88
Quartz	$SiO_2 \leftrightarrow SiO_{2(aq)}$	−4.00	−3.47	−3.15	22.69
Brucite	$Mg(OH)_2 + 2H^+ \leftrightarrow Mg^{2+} + 2H_2O$	16.30	14.27	13.20	24.54
Chlorite[a,b]	$(Mg_{2.964}Fe_{1.927}Al_{1.116}Ca_{0.011})(Si_{2.633}Al_{1.367})O_{10}(OH)_8 + 17.253H^+ \leftrightarrow 0.05375O_{2(g)} + 2.483Al^{3+} + 0.011Ca^{2+} + 1.927Fe^{2+} + 2.964Mg^{2+} + 12.6265H_2O + 2.633SiO_{2(aq)}$	59.41	48.21	40.06	211.92
CSH 0.8[a]	$Ca_{0.8}SiO_{2.8}{:}1.54H_2O + 1.6H^+ \leftrightarrow 0.8Ca^{2+} + 2.34H_2O + 1SiO_{2(aq)}$	11.05	10.19	9.58	59.29
CSH 1.2[a]	$Ca_{1.2}SiO_{3.2}{:}2.06H_2O + 2.4H^+ \leftrightarrow 1.2Ca^{2+} + 3.26H_2O + 1SiO_{2(aq)}$	19.30	17.70	16.33	71.95
CSH 1.6[a]	$Ca_{1.60}SiO_{3.6}{:}2.58H_2O + 3.2H^+ \leftrightarrow 1.6Ca^{2+} + 4.18H_2O + 1SiO_{2(aq)}$	28.00	25.59	23.94	84.68
Ettringite[a]	$Ca_6Al_2(SO_4)_3(OH)_{12}{:}26H_2O + 12H^+ \leftrightarrow 2Al^{3+} + 3SO_4^{2-} + 6Ca^{2+} + 38H_2O$	57.01	49.89	44.54	710.32
Gibbsite	$Al(OH)_3 + 3H^+ \leftrightarrow Al^{3+} + 3H_2O$	7.76	5.83	4.29	31.96
Hydrotalcite-CO_3[a]	$Mg_4Al_2[(OH)_{12}(CO_3)(H_2O)_2] + 13H^+ \leftrightarrow 2Al^{3+} + 1HCO_3^- + 4Mg^{2+} + 14H_2O$	61.20	51.77	45.26	301.51
Phillipsite	$K_{0.7}Na_{0.7}Ca_{1.1}(Al_{3.6}Si_{12.4})O_{32}{:}12.6H_2O + 14.4H^+ \leftrightarrow 0.7\,K^+ + 0.7Na^+ + 1.1Ca^{2+} + 3.6Al^{3+} + 12.4SiO_{2(aq)} + 19.8H_2O$	−6.76	−9.87	−11.72	609.20
Portlandite	$Ca(OH)_2 + 2H^+ \leftrightarrow 1Ca^{2+} + 2H_2O$	22.56	20.20	18.73	33.06
Saponite-Mg[a]	$Mg_3Si_4O_{10}(OH)_2 + 6H^+ \leftrightarrow 3Mg^{2+} + 4H_2O + 4SiO_{2(aq)}$	30.66	25.40	21.27	150.59
Talc	$Mg_3Si_4O_{10}(OH)_2 + 6H^+ \leftrightarrow 3Mg^{2+} + 4H_2O + 4SiO_{2(aq)}$	21.14	18.11	15.76	136.25
Tobermorite-11 Å	$Ca_5Si_6H_{11}O_{22.5} + 10H^+ \leftrightarrow 5Ca^{2+} + 6SiO_{2(aq)} + 10.5H_2O$	65.61	59.91	56.04	230.05

[a] Minerals imported from the database Thermoddem (http://thermoddem.brgm.fr/) compiled by BRGM.
[b] Thermodynamic properties published in [41].

Table 6
Kinetic constants used with each mineral.

Mineral	Reactive surface area ($m^2 \cdot m^{-3}$)	log k (25 °C)	n (60 °C)	n (90 °C)	E_a (kcal/mol)	Ref.
Primary minerals						
Albite	100	−15.6	−0.57	0	16.97	[42]
Calcite	100	−6	0	0	8.46	[42][a]
Cristobalite-α	100	−12.31	0	0	15.53	[42]
Illite	100	−11	0	0	15	[b]
K-feldspar	100	−12.7	0	0	10	[43][a]
Mg-montmor-FEBEX	100	−12.67	−0.5	−0.3	5.42	[40]
Quartz	100	−16.29	−0.55	0	25.88	[42]
Secondary minerals						
Brucite	100	−6	0	0	14.34	[44]
Chlorite	100	−8	0	0	10	[b]
CSH_0.8	100	−7	0	0	10	[40]
CSH_1.2	100	−7	0	0	10	[40]
CSH_1.6	100	−7	0	0	10	[40]
Ettringite	100	−8	0	0	10	[40]
Gibbsite	100	−10	0	0	15	[b]
Hydrotalcite-CO_3	100	−8	0	0	10	[b]
Phillipsite	100	−10	0	0	15	[b]
Portlandite	100	−8	0	0	10	[40]
Saponite-Mg	100	−11	0	0	15	[b]
Talc	100	−11	0	0	15	[b]
Tobermorite-11 Å	100	−10	0	0	10	[40]

The units of the kinetic constant (k) are given in $mol \cdot m^{-2} \cdot s^{-1}$.
[a] Kinetic parameters optimized from the given reference.
[b] Kinetic parameters assumed in this study.

The same specific surface area is assumed for all minerals (100 m^2 mineral$\cdot m^{-3}$ porous medium). Watson et al. [32] observed that the large relative abundance of montmorillonite minimized the dependency of modeling results on the surface area of other minerals. The model has an important kinetic component and the rate constants and exponents n have considerable leverage on the reactivity. These parameters are taken from experimental studies that include implicitly the contribution of the high surface areas of smectites. Dependency of reaction rates on pH at 60 °C has been considered for Mg-montmor-FEBEX, albite and quartz, and at 90 °C only for Mg-montmor-FEBEX (Table 6).

Against a general consensus that the dissolution rate of montmorillonite increases with increasing temperature, the justification for the chosen modification of the pH dependence from 60 to 90 °C is based on the observed decrease in the order of reaction in the transformation of montmorillonite at high pH. Sánchez et al. [13] described that the behaviour of the alkaline reaction is temperature dependent; therefore, at moderate temperatures (25–75 °C), the order of reaction is high (0.7), describing the partial dissolution of montmorillonite in the presence of precipitation of brucite. In the range of temperatures 125–200 °C, the order of reaction is lower (0.3) and montmorillonite transforms to saponite and zeolites. This latter reaction is complete and leads to the formation of silicate phases that capture Mg in the structure (i.e. the data represent apparent rates for the overall reaction, including precipitation). There is some agreement between this fact and our experimental results observed at 90 °C. The overall rate far from equilibrium (excluding the equilibrium term) at 90 °C is one order of magnitude smaller than at 60 °C, but also the pH is almost one order of magnitude lower at 90 °C. Brucite is scarcely observed but there is a change in the hydro-mechanical properties of the sample (hardening and clogging of porosity) and formation of interstratified chlorite–smectite at the interface. The chlorite-type phases observed experimentally (di-tri-octahedral or sudoite-type) are not available in the database, but instead a mixed di-tri-hydroxide (hydrotalcite) and Mg-silicates (talc and saponite) have been considered as a proxy.

At 90 °C, dependency of reaction rate on pH has only been considered for Mg-montmor-FEBEX. This assumption did not affect computed mass transfers but provided better numerical stability. It is emphasized that the montmorillonite dissolution rate is a rate-limiting parameter for the overall reaction progress, and the sensitivity of the system behaviour on the rates of secondary phases or minor primary phases is subordinate.

5. Results

The simulations have been performed at 60 and 90 °C, with YCW and ECW solutions for 360, 540 and 720 days (~12, 18 and 24 months).

5.1. YCW at 60 °C

Partial dissolution of Mg-montmor-FEBEX is observed in the first 3 mm of bentonite from the alkaline interface after 360 days and precipitation of secondary minerals in the same thickness (hydrotalcite, talc and brucite; Fig. 2). Tobermorite-11 Å precipitates <1% vol. in the first millimeter of the interface.

After 720 days dissolution of Mg-montmor-FEBEX increases at the interface with significant precipitation of the secondary minerals observed previously, however, the thickness of alteration remains (3–4 mm). This is related to the decrease of porosity in the altered area (Fig. 3).

While the mineralogical alteration is observed only in the first few millimeters from the alkaline interface, cation exchange processes are observed over the entire column of compacted bentonite. Exchangeable Mg^{2+} is displaced from the interlayer mainly by K^+ but also by Na^+ (Fig. 4). The total cation exchange capacity decreases as a function of time in the first 2–3 mm due to the partial dissolution of montmorillonite. Excess of Ca^{2+} and Mg^{2+} was measured experimentally in the medium of extraction of exchangeable cations (ammonium acetate at pH = 7), due to dissolution of calcite and Mg-hydroxides or Mg-amorphous phases. A correction for this measurement was performed considering that no exchangeable Ca^{2+} is present in bentonite in the YCW experiments and calculating the Mg^{2+}_{exch} as $CEC - \sum[Na^+_{exch} + K^+_{exch}]$. In the experiment there is no evidence for an increase of porosity in the first millimeters because bentonite at high density would swell to occupy any void space in the column.

5.2. YCW at 90 °C

Mineralogical results after 540 days show less alteration in the first millimeters compared to 60 °C and less montmorillonite dissolution (Fig. 5). Precipitation of secondary minerals extends to 10–11 mm. Brucite is the main product of reaction. A bit of hydrotalcite precipitates close to the reaction front (11 mm), and calcite and portlandite (<1% vol.) form in the first millimeter from the interface.

With the increase of temperature from 60 to 90 °C, the diffusion rates increase but the mineral dissolution rate of montmorillonite decreases (effect of n that dominates over the activation energy term). The net effect on the reactivity is observed as a more extended region of alteration with less geochemical transformations. This agrees with our hypothesis that at 90 °C the reaction is volumetrically more widespread but locally less intensive.

Hydrotalcite-CO_3 is a mixed hydroxide with the ideal formula $Mg_4Al_2[(OH)_{12}(CO_3)(H_2O)_2]$ that precipitates at the alteration front. In the model, it represents an interim phase that conserves parts of aluminum octahedral layers of montmorillonite. The model predicts almost exclusively precipitation of brucite at 90 °C, which in the experiment corresponds to the sum of several observed Mg-phases. Such slight differences between mineral stabilities in the Mg-system might be beyond what can be predicted from thermodynamic data,

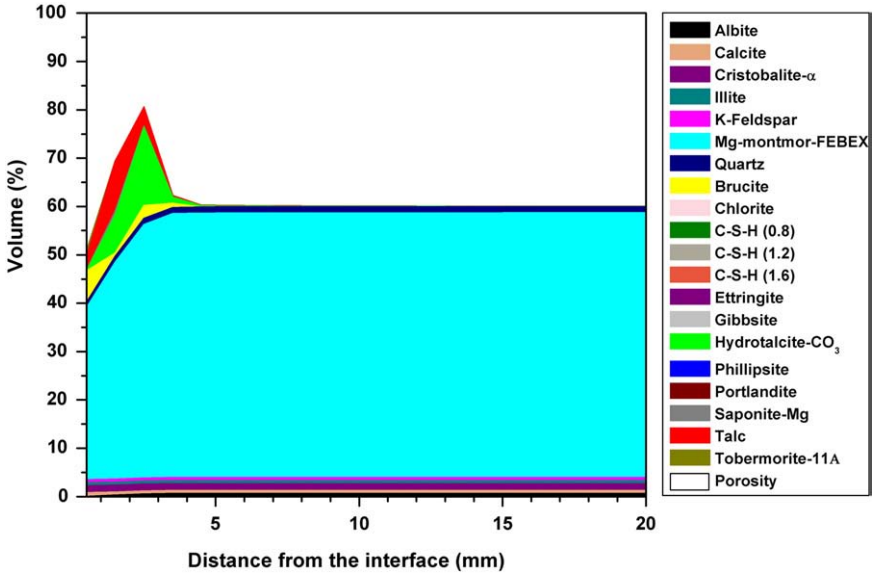

Fig. 2. Mineralogical distribution in the bentonite column interacting with the YCW solution at 60 °C after 360 days.

given their intrinsic uncertainties. Precipitation of brucite is directly related to cation exchange in montmorillonite. K^+ and Na^+ displace Mg^{2+} from the exchangeable region that precipitates as brucite. This is similar as in the case at 60 °C, but the model does not predict lower rates of exchange at 90 °C, as observed experimentally (Fig. 6). This is expected in the model because the rate of exchange depends directly on the multicomponent diffusion (higher at 90 °C). The experimentally observed textural effect (hardening) which is attributed to a distributed clogging effect cannot be represented in our numerical model. Watson et al. [32] obtained similar results as observed in the experiment at 60 °C for cation exchange by increasing the exchange rate of K^+ in their kinetic model.

The textural effects noted in the experiment may be attributed to the simulated mineralogical changes. If secondary minerals occupy more volume, the porosity decreases by the mineralogical transformation. This is supported by the measured lower BET surface areas in samples treated at 90 °C compared to 60 °C in regions apparently not affected by mineralogical alteration far from the alkaline interface. In the model, porosity at 90 °C decreases at a lower rate than at 60 °C in the first millimeters but extends further from the interface (12 mm after 540 days; Fig. 7).

5.3. ECW at 60 °C

The same physical parameters as in the case with YCW at 60 °C have been used in this model. The alkaline solution is now $Ca(OH)_2 = 0.02$ M which is oversaturated at $T > 25$ °C (saturation index of portlandite = 0.4667 at 60 °C). Mineralogical transformations are minor even after 720 days (Fig. 8). Mg-montmor-FEBEX dissolves only in the first millimeter from the interface, precipitating brucite (11% vol.), calcite (7% vol.), talc and hydrotalcite (~2% vol.), gibbsite and saponite-Mg (<0.2% vol.). Porosity decreases in the first millimeter from 40 to 20%. The most notable change predicted by the model is the ion exchange composition in montmorillonite. Ca^{2+} displaces Mg^{2+}

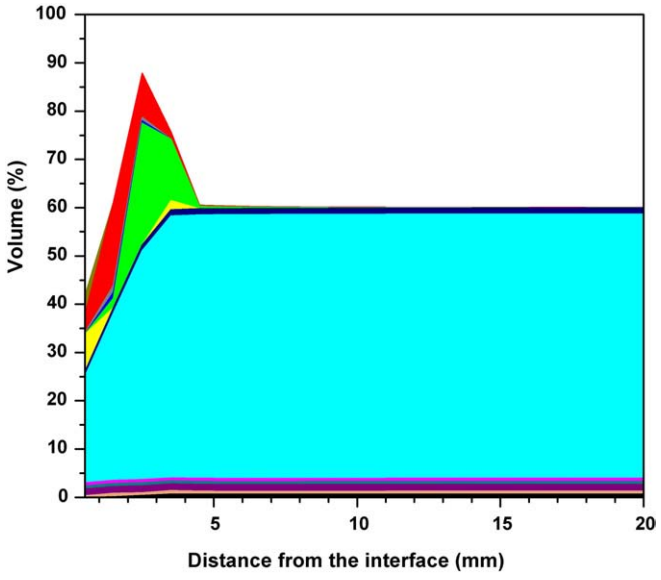

Fig. 3. Mineralogical distribution in the bentonite column interacting with the YCW solution at 60 °C after 720 days (legend shown in Fig. 2).

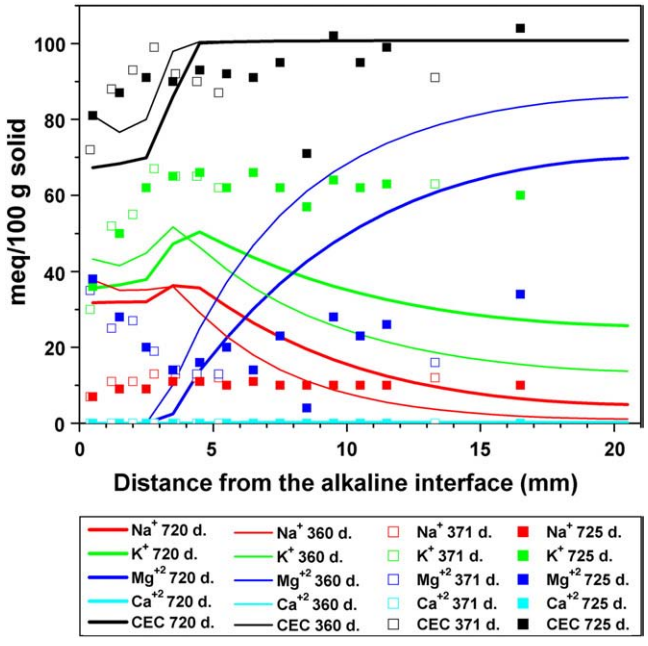

Fig. 4. Distribution of experimental exchangeable cations (squares) in bentonite at 60 °C after 12 and 24 months (YCW solution) and model prediction (lines).

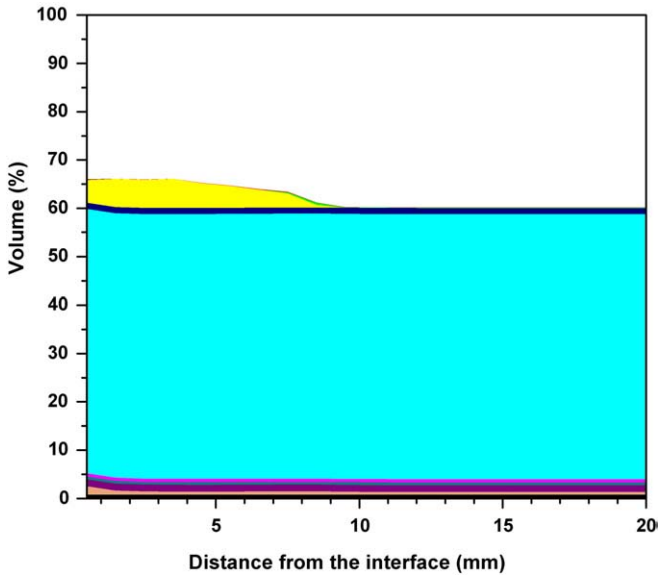

Fig. 5. Mineralogical distribution in the bentonite column interacting with the YCW solution at 90 °C after 540 days (legend shown in Fig. 2).

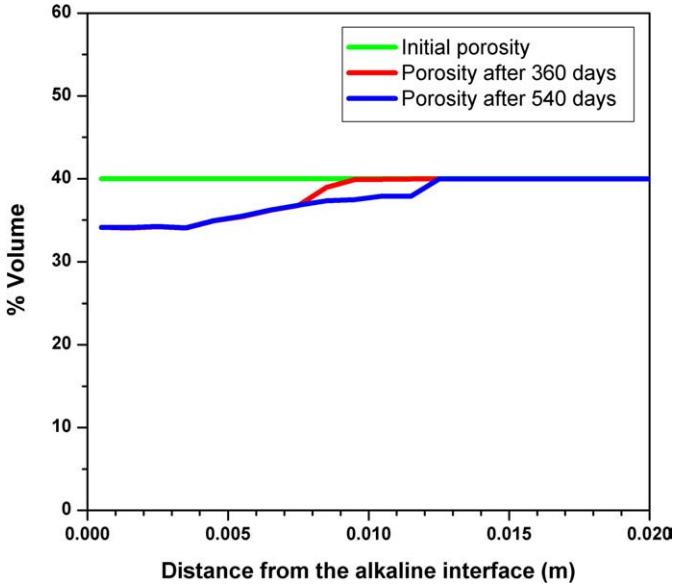

Fig. 7. Evolution of porosity in bentonite as a function of time (YCW solution at 90 °C).

significantly over the first 5 mm of bentonite (Fig. 9). The experimental observations show qualitatively exchange of Ca^{2+} for Mg^{2+} at the interface, but an excess of both cations (Ca^{2+} and Mg^{2+}) is measured in the medium of extraction for exchangeable cations. Since the same correction as performed for the YCW experiments is not valid in this case (Ca^{2+}_{exch} cannot be neglected), a detailed comparison of experimental and modeling data is not possible.

6. Discussion

The models predict that cation exchange in montmorillonite is the dominant process, which agrees with the experimental observations. Cation diffusion in the montmorillonite interlayer is favoured due to the high compaction of bentonite that reduces the fraction of free porewater and, therefore, the anion migration. Dead-end pores may have been formed in the system (porosity excluded from further reaction). As there is no advective transport, anion migration is subdued. There is enhanced ion migration in the region close to the alkaline interface, where montmorillonite is dissolving. If dissolution of primary minerals and precipitation of secondary minerals were considered in two sequential stages, aqueous species would be available and micropores connected when montmorillonite dissolves, creating an advective domain. However, precipitation of secondary phases reduces the porosity in the same region, decreasing the connection between the external alkaline fluid and the bentonite porewater. This inhibits the ionic diffusion in the column, mainly anionic (OH^-), able to dissolve montmorillonite. At 60 °C, a short altered region is observed at the interface (~2 mm) and the mineralogical alteration does not advance with time.

Since the dissolution rate of montmorillonite decreases with an increase of temperature (see further discussion), the mineralogical alteration at the interface is less at 90 °C than at 60 °C. Consequently, the porosity reduction is less pronounced and the alkaline plume extends farther. The model predicts the precipitation of brucite over

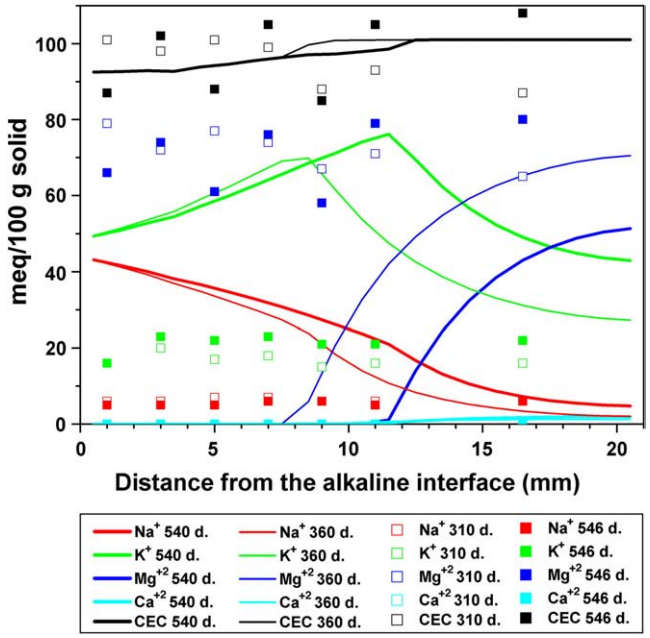

Fig. 6. Distribution of experimental exchangeable cations (squares) in bentonite at 90 °C after 12 and 18 months (YCW solution) and model prediction (lines).

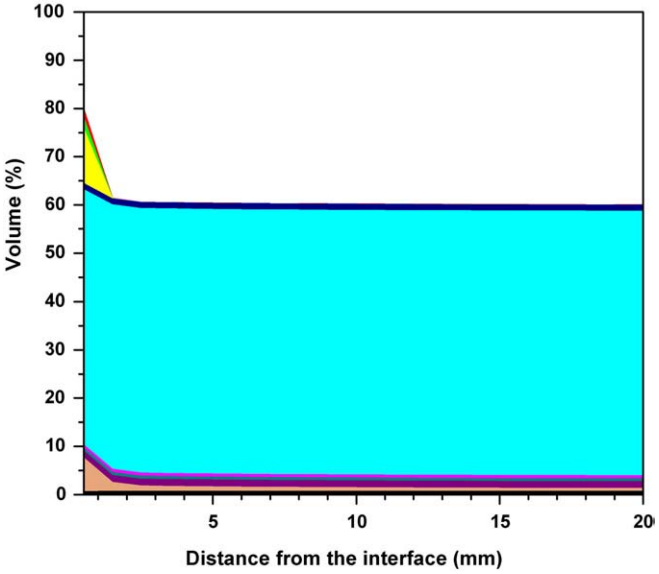

Fig. 8. Mineralogical distribution in the bentonite column interacting with the ECW solution at 60 °C after 720 days (legend shown in Fig. 2).

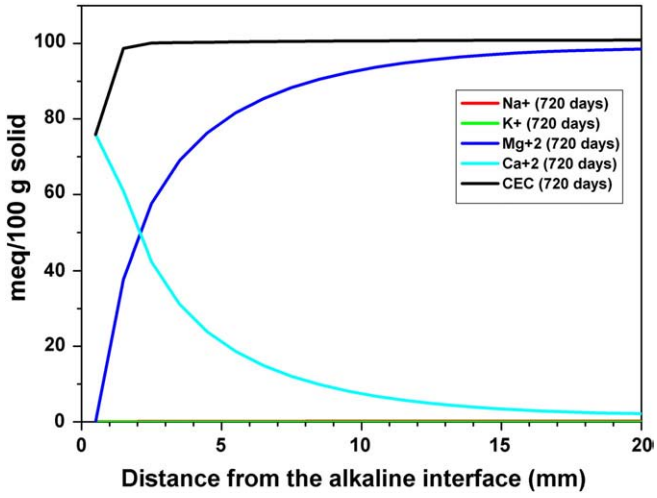

Fig. 9. Distribution of modeled exchangeable cations in bentonite at 60 °C after 720 days (ECW solution).

11 mm, but experimentally a hardening of the entire bentonite column was observed attributed to cementation processes. X-ray diffraction did not show significant changes in sequential samples taken parallel to the alkaline interface to study the mineralogical alteration, but this method may not be sensitive enough to indicate very minor transformations.

Applying Eq. (1) with $E_a = 5$ kcal·mol^{-1}, the diffusion coefficients for aqueous species increase as a function of temperature (Table 3). These diffusion coefficients are comparable to the effective diffusion coefficients used in similar studies with compacted bentonite, in the range 10^{-10}–10^{-11} m^2·s^{-1} according to the temperature applied 25–100 °C [48,49]; however, these coefficients consider implicitly retardation effects (tortuosity, surface adsorption, etc.) that are unknown *a priori* in the system and can only be estimated as a whole. One order of magnitude higher and lower diffusion coefficients were tested for this study; the results increased or decreased the reactivity significantly, loosing consistency with the experimental observations.

Precipitation of secondary minerals in bentonite needs to be interpreted coherently with the experimental results. Secondary mineral phases observed experimentally do not have a defined crystalline composition, and therefore, precipitation of talc, brucite and hydrotalcite must be considered as the result of Mg displacement from the exchange region in montmorillonite, with the eventual dissolution of montmorillonite and availability of Si, Al and other elements to form more stable phases in the specific geochemical conditions of reaction.

The alkaline alteration of bentonite in YCW experiments is heterogeneous and patches of unaltered bentonite have been detected at the interface, so Mg^{2+}_{exch} is still present at the interface. Exchange reactions are predicted by the model, but total displacement of Mg^{2+} by K^+ and Na^+ is calculated in the first millimeters from the interface. At higher temperature the exchange reactions are predicted to be more effective, in contrast with the experimental observations. This is mainly due to the faster diffusion, but again, the heterogeneity of bentonite has not been taken into account by the model. Obstruction of connected porosity, not exclusively at the interface but more distributed over the entire column of bentonite is suggested to explain the disagreement.

Another source of uncertainty, in addition to the lack of some thermodynamic data, is related to the kinetic parameters. Experimental studies on the rates of smectite dissolution at neutral or alkaline conditions disagree by several orders of magnitude (Table 7). These studies have been performed with high liquid (alkaline solution)/solid ratio, while the porewater/solid ratio for compacted bentonite is very low, and therefore, the kinetic constant for montmorillonite at the conditions of this experiment could be lower. In addition, it is remarkable that to better fit the model with the experimental results, the dependency of pH was decreased with the increasing temperature, based on the experimental observation reported by Sánchez et al. [13]. However, based on the Eq. (3), the montmorillonite dissolution rate increases with the increasing temperature, but the decrease of n offsets this effect, which is in disagreement with the general consensus. As observed in Table 7, reaction rates, activation energies and pH dependency may differ as a function of the experimental conditions used, and there are not yet validated kinetic parameters for the conditions used in the diffusion experiment modeled in this study. Therefore, a certain degree of flexibility was permitted to the kinetic values in order to achieve a model able to reproduce more closely the experimental results and support the interpretation of relevant processes. In this sense, the multicomponent diffusion process was a limiting factor to reach numerical convergence, and therefore, no sensitivity analysis could be performed on selected key parameters (such as the dissolution rate of montmorillonite). The modeling results and experimental evidences

Table 7
Literature data on kinetic of smectite dissolution in neutral and alkaline conditions (k in mol·m^{-2}·s^{-1}).

Reference	Experimental conditions	log k	E_a (Kcal/mol)	n	Remarks
Hayasi and Yamada [50]	Wyoming bentonite 80 °C pH = 10.5 Na_2CO_3 solution	−11.49			
Bauer and Berge [51]	Ceca and Ibeco bentonites 35–80 °C pH = 11.5–13.9 KOH 0.1–0.4 M solutions	−13.1			log k extrapolated to 13 °C pH = 10
Cama et al. [52]	FEBEX bentonite 80 °C pH = 8	−11.8			log k extrapolated to 25 °C pH = 13
Huertas et al. [53]	FEBEX bentonite 20, 40 and 60 °C 7.6 < pH < 8.5	−11.39 −12.31	7.29	−0.34	at pH < 8.0 at pH > 8.5
Sato et al. [54]	Kunipia P® bentonite 30, 50 and 70 °C pH = 8–13 I = 0.3 M (NaOH/NaCl − KOH/KCl)	−13.52 −13.85 −13.58	9.05 15.26	−0.27 −0.24 −0.15	70 °C 50 °C, pH = 8 30 °C, pH = 13
Sánchez et al. [13]	FEBEX bentonite 75–200 °C pH = 8.5–12.5 NaOH 0.1–0.5 M solutions	−12.12 −11.60 −11.38 −12.67	5.42	−0.7 −0.5 −0.3 −0.5	75 °C 125 °C 200 °C log k extrapolated to 25 °C; n fitted

suggest, however, that the pH dependence of the montmorillonite dissolution rate controls the mechanism of reactivity. In this respect, the alteration of bentonite by low-pH cements must be investigated within the framework of engineered barrier systems for deep geological disposal of radioactive waste.

Presently, kinetic parameters of reaction at alkaline conditions are still uncertain [15,23], so that a range of values must be assumed. In general, high rates of dissolution/precipitation can be assumed for simple minerals and those with less crystalline structures (carbonates, hydroxides and cement phases) and low reaction rates for those minerals with more complex and crystalline structures (clays and silicates). Large values have been assigned for minerals with fast reaction rates ($k_{25} = 10^{-6}$–10^{-10} mol·m^{-2}·s^{-1}) and low values for minerals with slower reaction rates ($k_{25} = 10^{-11}$–10^{-16}; see Table 6). These constants were used by Fernández et al. [40] to model long term alkaline alteration in FEBEX bentonite (except for illite, gibbsite, phillipsite, talc, chlorite and hydrotalcite).

Taking into account the model simulations performed by [32,40] and this study for a compacted FEBEX bentonite, it can be argued that:

1. The montmorillonite dissolution rate and the resultant precipitation of secondary minerals are temperature dependent.
2. The region of strong mineralogical transformation of bentonite is <5 mm; this region is reduced to 3 mm with the increase of dry density from 1.4 to 1.65 g·cm^{-3}.
3. The increase of temperature from 60 to 90 °C favours the extension of the reaction but does not produce a stronger mineralogical transformation.
4. Precipitation of zeolites at the interface has only been observed at pH >12 (measured at 25 °C) and temperatures over 90 °C.
5. Reactivity with Ca–OH fluids is not significant at the time scale used in the experiments. Mineralogical alteration is small but confirms cation exchange at the interlayer of montmorillonite.

7. Conclusions

The geochemical reactive transport models predict correctly, as seen experimentally, a porosity reduction within a mineralogical alteration zone of 2–3 mm when a highly concentrated alkaline solution (K–Na–OH) diffuses through a Mg-saturated compacted bentonite column.

The multicomponent diffusion model with higher coefficients for cations than for anions simulates the anion exclusion effect in compacted smectite-type clay materials and predicts that K^+ and Na^+ will diffuse rapidly from the alkaline source into bentonite displacing the exchangeable Mg^{2+}, that will be expelled from the montmorillonite interlayer to be incorporated in a non-exchange silicate.

The montmorillonite dissolution rate, which is temperature dependent, is an important factor in the overall reactivity. Extensive mineralogical alteration associated with porosity reduction is predicted in the first 2–3 mm from the interface at 60 °C. At 90 °C the dissolution rate for montmorillonite is lower and mineralogical transformations are less extensive but are more spread out in the column. Ca–OH fluids produce little alteration in the mineralogy of bentonite but exchange reactions are predicted in the interlayer of montmorillonite.

Textural effects observed in the experiment cannot be modeled but can be interpreted as precipitation of secondary minerals with larger molar volumes that reduce porosity. Also swelling effects are not considered that are a result of changing cation occupancy in the interlayers.

Bentonite alteration by high-pH solutions is a complex geochemical process operating at different scales controlled also by texture, and not the result of uniform reaction fronts as normally predicted by reactive transport models based on a homogeneous porous medium approach. We tried to reconcile the major mass transfer and mineral alteration processes by constraining the model with the experimental observations. While this has been reasonably successful it is also clear that one has to be careful in extrapolating such models to very long time scales. A significant aspect of this work is that the interlayer region may be modified to a significant depth, while the high-pH front is buffered effectively as generally accepted. While it is possible to further resolve the details of mineralogical transformations by carefully analyzed experiments, longer experimental times are clearly required to scale the results to repository conditions (time, dimensions, gradients, etc).

Acknowledgments

This work has been supported by ENRESA and the EU through contract FI6W-CT-2003-02389. Detailed comments by two anonymous reviewers are acknowledged and improved the clarity of the paper.

References

[1] U.R. Berner, Evolution of pore water chemistry during degradation of cement in a radioactive waste repository environment, Waste Management 12 (1992) 201–219.
[2] P. Faucon, F. Adenot, J.F. Jacquinot, J.C. Petit, R. Cabrillac, M. Jorda, Long-term behavior of cement pastes used for nuclear waste disposal: review of physico-chemical mechanisms of water degradation, Cement and Concrete Research 28 (6) (1998) 847–857.
[3] F.P. Glasser, M. Atkins, Cements in radioactive waste disposal, Materials Research Society Bulletin 12 (1994) 33–39.
[4] M. Adler, U.K. Mäder, H.N. Waber, High-pH alteration of argillaceous rocks: an experimental study, Schweizerische Mineralogische und Petrographische Mitteilungen 79 (3) (1999) 445–454.
[5] A. Bauer, B. Velde, Smectite transformation in high molar KOH solutions, Clay Minerals 34 (2) (1999) 259–273.
[6] J. Cuevas, R. Vigil, S. de la Villa, L.Sánchez Ramírez, R. Fernández, S. Leguey, The alkaline reaction of FEBEX bentonite: a contribution to the study of the performance of bentonite/concrete engineered barrier systems, Journal of Iberian Geology 32 (2) (2006) 151–174.
[7] R. Fernández, J. Cuevas, L. Sánchez, R. Vigil de la Villa, S. Leguey, Reactivity of the cement–bentonite interface with alkaline solutions using transport cells, Applied Geochemistry 21 (6) (2006) 977–992.
[8] U.K. Mäder, T. Fierz, B. Frieg, J. Eikenberg, M. Ruthi, Y. Albinsson, A. Mori, S. Ekberg, P. Stille, Interaction of hyperalkaline fluid with fractured rock: field and laboratory experiments of the HPF project (Grimsel Test Site, Switzerland), Journal of Geochemical Exploration 90 (1–2) (2006) 68–94.
[9] T. Melkior, D. Mourzagh, S. Yahiaoui, D. Thoby, J.C. Alberto, C. Brouard, N. Michau, Diffusion of an alkaline fluid through clayey barriers and its effect on the diffusion properties of some chemical species, Applied Clay Science 26 (1–4) (2004) 99–107.
[10] S. Nakayama, Y. Sakamoto, T. Yamaguchi, M. Akai, T. Tanaka, T. Sato, Y. Lida, Dissolution of montmorillonite in compacted bentonite by highly alkaline aqueous solutions and diffusivity of hydroxide ions, Applied Clay Science 27 (1–2) (2004) 53–65.
[11] S. Ramírez, Alteración alcalina hidrotermal de la barrera de bentonita por aguas intersticiales de cementos, PhD thesis, Universidad Autónoma de Madrid, Madrid, (2000), p 214.
[12] S. Ramirez, P. Vieillard, A. Bouchet, A. Cassagnabere, A. Meunier, E. Jacquot, Alteration of the Callovo-Oxfordian clay from Meuse–Haute Marne underground laboratory (France) by alkaline solution. I. A XRD and CEC study, Applied Geochemistry 20 (1) (2005) 89–99.
[13] L. Sánchez, J. Cuevas, S. Ramírez, D. Ruiz de León, R. Fernández, R. Vigil de la Villa, S. Leguey, Reaction kinetics of FEBEX bentonite in hyperalkaline conditions resembling the cement–bentonite interface, Applied Clay Science 33 (2) (2006) 125–141.
[14] W.R. Alexander, R. Dayal, K. Eagleson, J. Eikenberg, E. Hamilton, C.M. Linklater, I.G. McKinley, C.J. Tweed, A natural analogue of high pH cement pore waters from the Maqarin area of northern Jordan. II: results of predictive geochemical calculations, Journal of Geochemical Exploration 46 (1) (1992) 133–146.
[15] E.C. Gaucher, P. Blanc, Cement/clay interactions — a review: experiments, natural analogues, and modeling, Waste Management 26 (7) (2006) 776–788.
[16] I.G. McKinley, Applying Natural Analogues in Predictive Performance Assessment, U. N. I. Report Ed. Nagra, Wettingen, Switzerland, 1989.
[17] A.E. Milodowski, J.M. Pearce, C.R. Hughes, H.N. Khoury, A Preliminary Mineralogical Investigation of a Natural Analogue of Cement-buffered Hyperalkaline Groundwater Interaction with Marl, Maquarin, northern Jordan, Nagra report NIB 92-50, Wettingen, Switzerland, 1992.
[18] J.A.T. Smellie, W.R. Alexander, P. Degnan, L. Griffault, U.K. Mader, L. Trotignon, The role of the Jordan natural analogue studies in the performance assessment of cementitious repositories for radioactive wastes, Water–Rock Interaction,

Proceedings of the International Symposium on Water–Rock Interaction, 10th, Villasimius, Italy, 2, 2001, pp. 1391–1393.
[19] J.A.T. Smellie, F. Karlsson, W.R. Alexander, Natural analogue studies: present status and performance assessment implications, Journal of Contaminant Hydrology 26 (1–4) (1997) 3–17.
[20] L. De Windt, D. Pellegrini, J. van der Lee, Coupled modeling of cement/claystone interactions and radionuclide migration, Journal of Contaminant Hydrology 68 (3–4) (2004) 165–182.
[21] E.C. Gaucher, P. Blanc, J.-M. Matray, N. Michau, Modeling diffusion of an alkaline plume in a clay barrier, Applied Geochemistry 19 (10) (2004) 1505–1515.
[22] U.K. Mäder, D. Traber, Reactive transport model of cement–clay stone interaction with application to a HLW repository in Opalinus Clay, Final Report of the ECOCLAY-II Project, E. Commission Ed, 2004, pp. 285–291.
[23] D. Savage, D. Noy, M. Mihara, Modeling the interaction of bentonite with hyperalkaline fluids, Applied Geochemistry 17 (3) (2002) 207–223.
[24] J.M. Soler, U.K. Mäder, Interaction between hyperalkaline fluids and rocks hosting repositories for radioactive waste: reactive transport simulations, Nuclear Science and Engineering 151 (1) (2005) 128–133.
[25] P. Wersin, Geochemical modeling of bentonite porewater in high-level waste repositories, Journal of Contaminant Hydrology 61 (1–4) (2003) 405–422.
[26] K. Yokozeki, K. Watanabe, N. Sakata, N. Otsuki, Modeling of leaching from cementitious materials used in underground environment, Applied Clay Science 26 (1–4) (2004) 293–308.
[27] R. Fernández, U.K. Mäder, M. Rodríguez, R. Vigil de la Villa, J. Cuevas, Alteration of compacted bentonite by diffusion of highly alkaline solutions, European Journal of Mineralogy (2009), doi:10.1127/0935-1221/2009/0021-1947.
[28] S. Ramírez, J. Cuevas, R. Vigil, S. Leguey, Hydrothermal alteration of "La Serrata" bentonite (Almeria, Spain) by alkaline solutions, Applied Clay Science 21 (5–6) (2002) 257–269.
[29] C.I. Steefel, GIMRT, version 1.2: Software for Modeling Multicomponent, Multidimensional Reactive Transport, User's Guide, UCRL-MA-143182, Lawrence Livermore National Laboratory: Livermore, California, 2001.
[30] C.I. Steefel, CrunchFlow. Software for Modeling Multicomponent Reactive Flow and Transport, User's manual., E. S. Division Ed. Lawrence Berkeley National Laboratory: Berkeley, CA, 2006, p. 82.
[31] C.I. Steefel, S.B. Yabusaki, OS3D/GIMRT, Software for multicomponent-Multidimensional Reactive Transport: User's Manual and Programmer's Guide, P. N. N. L. Report PNL-11166 Ed. Richland, Washington, 1996, p. 58.
[32] C.E. Watson, K. Hane, D. Savage, S.J. Benbow, J. Cuevas, R. Fernández, Reaction and diffusion of cementitious water in bentonite: results of 'blind' modelling, Applied Clay Science 45 (2009) 54–69.
[33] S.J. Benbow, C.E. Watson, Raiden 3 User Guide, Q. R. QRS-1259A-1 Ed, Quintessa Ltd, UK, 2004.
[34] F.J. Huertas, P. Carretero, J. Delgado, J. Linares, J. Samper, An experimental study on the ion-exchange behavior of the smectite of Cabo de Gata (Almeria, Spain): FEBEX bentonite, Journal of Colloid and Interface Science 239 (2) (2001) 409–416.
[35] C.A.J. Appelo, P. Wersin, Multicomponent diffusion modeling in clay systems with application to the diffusion of tritium, iodide, and sodium in opalinus clay, Environmental Science and Technology 41 (14) (2007) 5002–5007.
[36] A.M. Fernández, B. Baeyens, M. Bradbury, P. Rivas, Analysis of the porewater chemical composition of a Spanish compacted bentonite used in an engineered barrier, Physics and Chemistry of the Earth 29 (2004) 105–118.
[37] I.C. Bourg, A.C.M. Bourg, G. Sposito, Modeling diffusion and adsorption in compacted bentonite: a critical review, Journal of Contaminant Hydrology 61 (1–4) (2003) 293–302.
[38] K.R. Applin, The diffusion of dissolved silica in dilute aqueous solution, Geochimica et Cosmochimica Acta 51 (8) (1987) 2147–2151.
[39] Y.-H. Li, S. Gregory, Diffusion of ions in sea water and in deep-sea sediments, Geochimica et Cosmochimica Acta 38 (5) (1974) 703–714.
[40] R. Fernández, J. Cuevas, U.K. Mäder, Modelling concrete interaction with a bentonite barrier, European Journal of Mineralogy 21 (2009) 177–191.
[41] H. Gailhanou, J. Rogez, J.C. v. Miltenburg, A.C.G. v. Genderen, J.M. Grenèche, C. Gilles, D. Jalabert, N. Michau, E.C. Gaucher, P. Blanc, 4738–4749, Thermodynamic properties of chlorite CCa-2. Heat capacities, heat contents and entropies, Geochimica et Cosmochimica Acta 73 (16) (2009) 4738–4749.
[42] J.L. Palandri, Y.K. Kharaka, A compilation of rate parameters of water–mineral interaction kinetics for application to geochemical modelling, U. S. Geological Survey open file report 2004-1068, 2004, p. 74.
[43] P. Schweda, Kinetics of alkali feldspar dissolution at low temperature, Proceedings of the 6th International Symposium on Water–Rock Interaction, 1989, pp. 609–612, Vol. WRI-6.
[44] G. Jordan, W. Rammensee, Dissolution rates and activation energy for dissolution of brucite (001): a new method based on the microtopography of crystal surfaces, Geochimica et Cosmochimica Acta 60 (24) (1996) 5055–5062.
[45] A.C. Lasaga, Rate laws of chemical reactions, Reviews in Mineralogy 8 (1981) 1–68.
[46] A.C. Lasaga, Chemical kinetics of water–rock interactions, Journal of Geophysical Research, B 89 (B6) (1984) 4009–4025.
[47] P. Aagaard, H.C. Helgeson, Thermodynamic and kinetic constraints on reaction rates among minerals and aqueous solutions. I. Theoretical considerations, American Journal of Science 282 (3) (1982) 237–285.
[48] J. Lehikoinen, T. Carlsson, A. Muurinen, M. Olin, P. Salonen, Evaluation of factors affecting diffusion in compacted bentonite, Materials Research Society Symposium Proceedings, (Scientific Basis for Nuclear Waste Management XIX), 412, 1996, pp. 675–682.
[49] G. Montes-H, B. Fritz, A. Clement, N. Michau, Modeling of transport and reaction in an engineered barrier for radioactive waste confinement, Applied Clay Science 29 (3–4) (2005) 155–171.
[50] H. Hayashi, M. Yamada, Kinetics of dissolution of noncrystalline oxides and crystalline clay minerals in a basic Tiron solution, Clays and Clay Minerals 38 (1990) 308–314.
[51] A. Bauer, G. Berger, Kaolinite and smectite dissolution rate in high molar KOH solutions at 35 Deg and 80 DegC, Applied Geochemistry 13 (7) (1998) 905–916.
[52] J. Cama, J. Ganor, C. Ayora, C.A. Lasaga, Smectite dissolution kinetics at 80 C and pH 8.8, Geochimica et Cosmochimica Acta 64 (15) (2000) 2701–2717.
[53] F.J. Huertas, E. Caballero, C. Jimenez, F. de Cisneros, J.Linares Huertas, Kinetics of montmorillonite dissolution in granitic solutions, Applied Geochemistry 16 (4) (2001) 397–407.
[54] T. Sato, M. Kuroda, S. Yokoyama, M. Tsutsui, K. Fukushi, T. Tanaka, S. Nakayama, Dissolution mechanism and kinetics of smectite under alkaline conditions, Proceedings of Joint NUMO-Posiva International Workshop on Bentonite–Cement Interaction in Repository Environments, 2004.